PRISTINE CR2 CAIs PRESERVE INITIAL ABUNDANCES OF SHORT-LIVED RADIONUCLIDES ^{10}Be AND ^{26}Al. E.T. Dunham[1], M. Wadhwa[1], M.-C. Liu[2], A.T. Hertwig[2], N. Kita[3], K. Fukuda[3], D.L. Schrader[1], J. Davidson[1]. [1]Center for Meteorite Studies, Arizona State University, Tempe, AZ 85287 (etdunham@asu.edu), [2]Dept. of Earth, Planetary, and Space Sciences, University of California, Los Angeles, CA 90095, [3]Dept. of Geoscience, University of Wisconsin, Madison, WI 53706.

Introduction: Beryllium-10, which decays to ^{10}B with a half-life of 1.4 Ma, is produced almost exclusively by non-thermal nuclear reactions induced by solar energetic particles and galactic cosmic rays (e.g., [1]). The initial abundance of this short-lived radionuclide (SLR) can be inferred from the slope of the correlation between ^{10}B/^{11}B and ^{9}Be/^{11}B in calcium- aluminum-rich inclusions (CAIs), the first-formed solids in the early Solar System. The inferred initial ^{10}Be/^{9}Be is in the range of ~(6-100)×10^{-4} with most CAIs having a value ~8×10^{-4} [2-10]. Although there are many models explaining ^{10}Be formation [2,5,10-13], the wide range in its initial abundance suggests that CAIs or their precursors were irradiated stochastically in the hot midplane of the disk (as opposed to in the molecular cloud [13]).

Studies of ^{10}Be-^{10}B isotope systematics in CAIs can provide insights into the astrophysical environment of the early Solar System. However, most CAIs studied thus far have been from CV3 chondrites (because they are relatively abundant and large) that are known to have undergone extensive parent body aqueous alteration and thermal metamorphism [14]. CR2 (Renazzo-type) chondrites, on the other hand, are among the least metamorphosed [15]. In spite of CR2 CAIs being mineralogically pristine, they have not been extensively studied for their isotopic compositions as they are typically quite small (<500 μm). Indeed, only a handful of CR2 CAIs have been studied for ^{26}Al-^{26}Mg and oxygen isotope systematics [15,16]. Here we report for the first time the results of an investigation of ^{10}Be-^{10}B isotope systematics in several CR2 CAIs.

Correlations between the initial abundances of ^{10}Be and ^{26}Al can provide valuable information about the age and thermal history of CAIs (e.g., [4]). Therefore, in this study, we additionally investigated the ^{26}Al-^{26}Mg isotope systematics in selected CR2 CAIs in which we determined ^{10}Be-^{10}B isotope systematics.

Methods: Several CAIs in carbon coated thin sections of four CR2 chondrites (two CAIs in MIL 090657,6 [17], two in LAP 02342,14 [18], three in Shişr 033 [19], and one in NWA 801 [18]) were characterized using the JEOL JXA-8530F at Arizona State University (ASU). The ^{10}Be–^{10}B isotope systematics in these eight CAIs were determined using the IMS-1290 secondary ion mass spectrometer (SIMS) at UCLA with a 5−10 nA $^{16}O^-$ primary beam (beam diameter ~5−10 μm, generated by a *Hyperion-II* source [20]). Secondary ion intensities were measured with multiple electron multipliers (EMs) with a mass resolving power of ~2,500 in dynamic multicollection mode. A NIST 614 glass was used as a standard to obtain the ^{9}Be/^{11}B relative sensitivity factor (RSF), and the ^{10}B/^{11}B instrumental mass fractionation (IMF) [21].

Three of the eight CAIs were additionally chosen for ^{26}Al–^{26}Mg isotope measurements using the IMS-1280 SIMS at UW-Madison. We measured melilite, spinel, and anorthite in the interior of the CAIs, and diopside and anorthite in the CAI rims (when present). Due to the small size (~3 μm) of the anorthite grains in one of the samples, we made FIB marks [22] with the Nova 200 NanoLab FEI at ASU. These marks on the carbon coat above candidate grains were later located with a SIMS $^{27}Al^+$ raster ion image. For anorthite spot analyses, we used a 20 pA $^{16}O_2^-$ beam to produce a 2 μm spot, and measurements were made in monocollection EM mode. The analyses on melilite, spinel, and pyroxene were made with Faraday cups (with three 10^{12} ohm amplifiers for Mg isotopes) in multicollection mode, with a beam current that varied from 0.5 to 2 nA to produce 5-12 μm spots. Data reduction procedures including calibration of standards are in [23].

Results: *Sample Petrography.* The eight CAIs vary in their texture, mineralogy, and size (length of the longest axis). CAIs *Cereus* (0.4 mm) and *Hibiscus* (0.2 mm) from LAP 02342 are both rounded melilite-rich igneous inclusions. CAIs *Creosote* (0.9 mm) and *Yucca* (1 mm) from MIL 090657 are both rounded, fragmented, partially rimmed igneous inclusions; *Creosote* is predominately melilite while *Yucca* is nearly equal parts melilite, fassaite, and spinel. CAI *Dalea* (0.2 μm) from Shişr 033 is a rounded melilite-rich igneous inclusion with a thick diopside rim while CAIs *Rosewood* (2.3 mm) and *Sonoran* (1.7 mm) are irregularly shaped condensate spinel-pyroxene aggregates. CAI *Palo Verde* (0.3 mm) in NWA 801 is an irregularly shaped melilite grain.

^{10}Be–^{10}B Isotope Systematics. Four of the eight CAIs (*Cereus, Yucca, Dalea,* and *Palo Verde*) showed resolvable excesses in radiogenic ^{10}B correlated with

^{9}Be/^{11}B that correspond to similar inferred initial ^{10}Be/^{9}Be ratios within the errors. Taken together, they record a weighted average ^{10}Be/^{9}Be = (7.7±1.3)×10^{-4} (2σ errors). As an example, the data for *Yucca* and *Dalea* are shown in Fig. 1. Only upper limits on the initial ^{10}Be/^{9}Be could be inferred for the other four CAIs (*Hibiscus*, Creosote, *Rosewood*, and *Sonoran*) because they did not show any resolvable radiogenic ^{10}B excesses. Taken together, they define an upper limit on the initial ^{10}Be/^{9}Be of ≤8.6×10^{-4}, which is nevertheless consistent with the inferred initial ^{10}Be/^{9}Be of ~8×10^{-4} in the other four CAIs. As an example, the data for *Creosote* are shown in Fig. 1.

^{26}Al–^{26}Mg Isotope Systematics. The CAIs *Dalea*, *Yucca,* and *Creosote* are found to have the same initial ^{26}Al/^{27}Al within uncertainties (Fig. 2), with values in the range of (4.4-4.7)×10^{-5}.

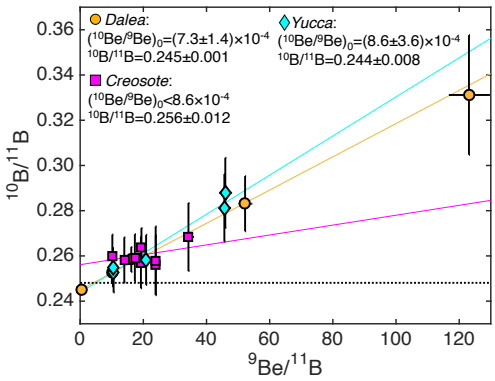

Fig. 1: The ^{10}Be-^{10}B isochrons for the CAI *Dalea* from Shişr 033 and the CAIs *Yucca* and *Creosote* from MIL 090657. The horizontal line indicates the chondritic ^{10}B/^{11}B ratio [24]. Error bars are 2σ

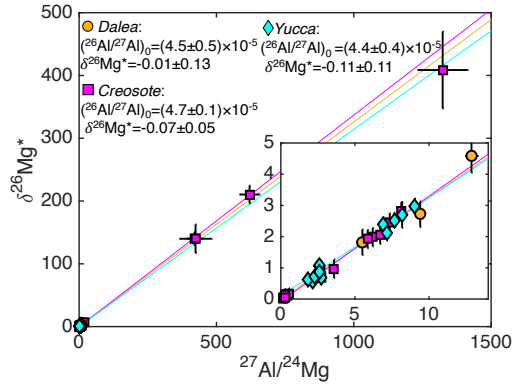

Fig. 2: The ^{26}Al-^{26}Mg isochrons for the CAI *Dalea* from Shişr 033 and the CAIs *Yucca* and *Creosote* from MIL 090657. The inset plot shows spinel, pyroxene, and melilite data. Error bars are 2σ.

Discussion: The three CAIs *Dalea*, *Yucca,* and *Creosote* for which both ^{10}Be–^{10}B and ^{26}Al–^{26}Mg isotope systematics were determined are typical of melilite-rich CAIs from CR2 chondrites, although they are slightly larger than average [15,16]. The ^{26}Al/^{27}Al recorded in these CAIs falls within the range reported previously in CR2 CAIs of (4.5−5.0)×10^{-5} [15]. This suggests that CR2 CAIs formed within ~0.5 Ma of CAIs with the canonical ^{26}Al/^{27}Al ratio [15].

If ^{26}Al-poor and CH/CB CAIs are not included, about 75% of CAIs measured (predominately CV3 CAIs including all geochemical-petrologic types) record a range in inferred ^{10}Be/^{9}Be of (5−12)×10^{-4}. The weighted average value of ^{10}Be/^{9}Be for this data set (n=27) is (7.2±0.2)×10^{-4} [2-10]. It is remarkable that the weighted average ^{10}Be/^{9}Be of (7.7±1.3)×10^{-4} in the CR2 CAIs studied here matches so closely with the weighted average of the majority of previously measured CAIs. This suggests that, on average, most CAIs or their precursors received a similar dose (~1×10^{19} cm^{-2} [11]) of energetic particles within the first ~0.5 Ma of Solar System history, independent of the chondrite classes in which they were found.

A few outlier CAIs from CV3 chondrites are inferred to have ^{10}Be/^{9}Be ~(12−70)×10^{-4} [10,21]. This suggests the while the fluence of high energy particles in the main CAI forming region was nearly uniform, some CAIs nevertheless experienced a higher fluence. Another possible explanation for the apparently higher ^{10}Be/^{9}Be in some CV3 CAIs is that this may be the result of secondary processes on the CV3 parent body.

Acknowledgments: This work is supported by a NASA Earth and Space Science Fellowship (NNX16AP48H) to ETD and a NASA Emerging Worlds grant (NNX15AH41G) to MW.

References: [1] Davis A.M. & McKeegan K.D. (2014), *Treatise on Geochemistry (2nd Ed.),* p.361. [2] McKeegan K.D. et al. (2000) *Science 289,* 1334. [3] Sugiura N. et al. (2001) *MAPS 36,* 1397. [4] MacPherson G.J. et al. (2003) *GCA 67,* 3165. [5] Chaussidon M. et al. (2006) *GCA 70,* 224. [6] Liu M.-C. et al. (2009) *GCA 73,* 5051. [7] Wielandt D. et al. (2012) *ApJ 748,* 25. [8] Gounelle M. et al. (2013) *ApJ 763,* 33. [9] Srinivasan G. et al. (2013) *EPSL 374*, 11. [10] Sossi P.A. et al. (2017) *Nature Astronomy 1*, 0055 [11] Tatischeff V. et al. (2014) *ApJ 796*, 124. [12] Bricker G.E. and Caffee M.W. (2010) *ApJ 725*, 443. [13] Desch S.J. et al. (2004) *ApJ 602*, 528. [14] Krot A.N. et al. (1998) *MAPS 33*, 1065. [15] Makide K. et al. (2009) *GCA 73*, 5018. [16] Aléon J. et al. (2002) *MAPS 37*, 1729. [17] Davidson J. et al. (2015) *LPS 46,* #1603. [18] Schrader D.L. et al. (2011) *GCA 75*, 308. [19] Schrader D.L. et al. (2015) *MAPS 50*, 15. [20] Liu M.-C. et al. (2018) *IJMS*, 1-9. [21] Dunham E.T. et al. (2018) *LPS 49,* #2402. [22] Defouilloy C. et al. (2017) *EPSL 465*, 145. [23] Ushikubo T. et al. (2017) *GCA 201*, 103. [24] Zhai M. et al. (1996) *GCA 60*, 4877.